Journal of Thermal Analysis and Calorimetry
https://doi.org/10.1007/s10973-024-13172-x

Case study on thermal management of planar elements with various polymeric heat exchangers: experiment and simulation

Jiri Hvozda[1] · Krystof Mraz[1] · Miroslav Raudensky[1] · Alexander Vakhrushev[2] · Ebrahim Karimi-Sibaki[2] · Jan Bohacek[1]

Received: 18 July 2023 / Accepted: 4 April 2024
© The Author(s) 2024

Abstract

A reliable battery thermal management system (BTMS) is essential to ensure proper performance, a long life span and high electric vehicle safety. The primary objective of BTMS is to maintain the cells' temperature in the range of 15–35 °C while limiting the temperature spread between cells to below 5 °C. Active thermal management with polymeric hollow fibers (PHFs) has been reported in a few articles, but its tremendous flexibility is mainly advantageous for cylindrical cells. Extruded polymeric cold plate heat exchangers with rounded rectangle channels (RRCs) are proposed as a more elegant solution for planar batteries. Heat exchangers using PHFs and RRCs were experimentally compared, with a strong focus on minimizing the maximum temperature and temperature spread of the experimental setup while simultaneously achieving minimal pressure drops. The system behavior with different parameters, including materials, geometry and thermophysical properties, was further studied using properly validated CFD models.

Keywords Battery thermal management systems · Heat exchangers · Planar batteries · Polymeric cold plates · Polymeric hollow fibers

Introduction

According to the International Energy Agency, the number of electric cars on the world's roads in 2010 was only around 17000. However, by the end of 2021, this number had skyrocketed to nearly 17 million. Despite the global downturn in car sales caused by the pandemic, electric car registrations saw a remarkable 41% increase in 2020, while overall global car sales dropped by 16%. In 2020, approximately 3 million electric cars were sold worldwide, accounting for a sales share of 4.6%. This figure further rose to over 6.5 million in 2021, representing a sales share of 10%. Additionally, the cost of batteries has decreased by more than 85% since 2010. Electric vehicles (EVs) are crucial in reducing air pollution in densely populated areas and offer a promising solution for energy diversification and reducing greenhouse gas emissions. EVs produce zero tailpipe emissions and demonstrate better efficiency than internal combustion engines. Combined with a low-carbon electricity sector, they have significant potential for reducing greenhouse gas emissions. These factors strongly indicate that the 2020s will witness a significant expansion in electric mobility [1, 2].

One of the major challenges in electromobility is battery thermal management, which significantly impacts battery performance, safety and life span [3, 4]. Temperature variations caused by heat generation within the battery can lead to various undesired effects such as capacity and power fade, self-discharge and electrical imbalance. Maintaining battery system temperature in the range of 15–35 °C is crucial to ensure optimal battery performance, lifetime and safety. Keeping temperature uniformity within 5 °C is also essential [5, 6]. Battery thermal management systems (BTMS) are classified into passive, active and hybrid groups [7, 8]. Passive methods, such as immersion in liquid, natural air convection, heat pipes or phase change materials (PCMs), offer energy efficiency and durability but may not be suitable

✉ Jiri Hvozda
Jiri.Hvozda@vut.cz

[1] Heat Transfer and Fluid Flow Laboratory, Faculty of Mechanical Engineering, Brno University of Technology, Antoninska 548/1, 60190 Brno, Czechia

[2] Christian-Doppler Laboratory for Metallurgical Applications of Magnetohydrodynamics, Department of Metallurgy, Montanuniversitaet Leoben, Franz-Josef Strasse 18, 8700 Leoben, Austria

Published online: 02 May 2024

for long-term use in EVs [9–13]. Active methods provide high-performance efficiency and safety, including forced air and liquid flow. Also, liquid BTMS stands out as a more compact option. Hybrid systems combine active and passive approaches but are limited in their use due to complexity and cost [14–17]. Currently, most EVs utilize active liquid or air BTMS, with active liquid systems employed by TESLA and Volkswagen. At the same time, Toyota, Hyundai, Nissan and Renault primarily use active air BTMS. Further research should focus on optimizing active BTMS, as it offers a reasonable balance between cost and effectiveness. However, the best arrangements and optimal operating conditions for BTMS are still to be determined.

Existing BTMS predominantly utilizes metals such as aluminum and copper, which come with a significant carbon footprint. In contrast, proposed polymeric materials offer a much more environmentally friendly alternative. For instance, extruded polypropylene generates approximately five times less CO_2 per kilogram than extruded aluminum. Additionally, polymers possess the advantages of being lightweight and electrically non-conductive. The low thermal conductivity of polymers can be partially addressed by incorporating graphite or designing thin walls for the heat exchangers (HEs) [18, 19]. Unlike metal HEs that require additional (polymeric) electrical insulators to prevent short circuits, polymeric counterparts eliminate the need for such insulation. Notably, the thickness of these electrical insulators is typically equal to the wall thickness of the polymeric heat exchanger (PHE). Consequently, the marginal benefit of highly conductive materials like aluminum becomes negligible [20, 21].

Zarkadas and Sirkar introduced polymeric hollow fiber heat exchangers (PHFHEs) in 2004 [22]. These PHFHEs have been successfully used in thermal management for cylindrical Li-ion 18,650 cells. By embedding polypropylene hollow fibers with an inner diameter of 0.84 mm into a durable polydicyclopentadiene housing, the module achieved comparable temperature performance to the TESLA S battery unit [23, 24]. In a 2021 prototype improvement, the fibers were redesigned to have direct contact with the cells, and the inlet/outlet manifolds were improved for flexibility. Multiple heat exchangers were assembled to fill the space between the cells, providing a heat exchanger-to-battery mass-weighted ratio of about 1:5. With a coolant flow rate of 45 mL min^{-1} and discharging at a constant current that discharged the whole battery in 1 hour, the achieved temperature of 22 °C with a temperature spread of 4 °C met the BTMS requirements [20]. Due to their flexibility, large heat transfer area and chemical resistance, PHFHEs have demonstrated feasibility in various fields, including desalination, automotive applications and air-conditioning [25–29].

Most current EVs seem to have planar cells (prismatic and pouch). Thus, the exceptional flexibility of the fibers is unimportant. Furthermore, PHFHE manufacturing is expensive to scale up. Only one channel (a fiber, respectively) is extruded at the time. Thus, more extrusion machines are required, or the production of a HE takes too much time. More importantly, when it comes to the thermal management of planar elements with fibers (i.e., tubes), a significant issue arises due to inadequate physical contact between them. Hence, a considerable amount of thermally conductive paste is required. To preserve the advantages of PHFs and overcome the issue with fiber geometry, authors propose the usage of PHEs with a flat surface and rounded rectangular channels (RRCs)—polymeric cold plate heat exchangers (PCPHE). The inspiration comes from the commercially used plastic cardboard used in logistics. Plastic cardboard is also like fibers manufactured by extrusion. However, unlike them, the whole board is extruded at once (i.e., all channels in cardboard are extruded simultaneously), which enhances production scalability.

Current technology and materials to produce plastic cardboard are not yet optimal for heat transfer long-term applications. Cheap polypropylene has to be replaced with a heat-stabilized polymer. Further, the cardboard's dimensions and shape must be reconsidered to improve its mechanical stability, which is required by external loading from batteries. An experimental comparison of two thermal management approaches (PHFHE and PCPHE) of planar elements was carried out with planar dummy cells maintained at constant power. The experiments were also used to validate a numerical model, which was further used to study the system with different parameters such as geometry and thermophysical properties.

Methodology

Experimental description

Two heat exchangers were produced. The first one (further in the text denoted as *F*) used 180 hollow fibers made of polyamide with a length of 140 mm, 1 mm outer diameter and 0.8 mm inner diameter, placed in a single layer (Fig. 1a). Polyamide (PA) encompasses a broad spectrum of materials, with PA6 and PA11 being the most commonly used in technical applications. The fibers examined in this research were produced using PA 612 (Zytel 6159). PA 612 is easily processable by extrusion and by following the melt drawing to the required dimension of the hollow fiber. The melt temperature range by extrusion is 230–250 °C. Fiber extrusion was performed by the company COMPUPLAST s.r.o.

The second HE (*C*) was made from plastic cardboard, commonly used as a support or protection when transporting materials. It contains 61 channels (Fig. 1b). The heat transfer

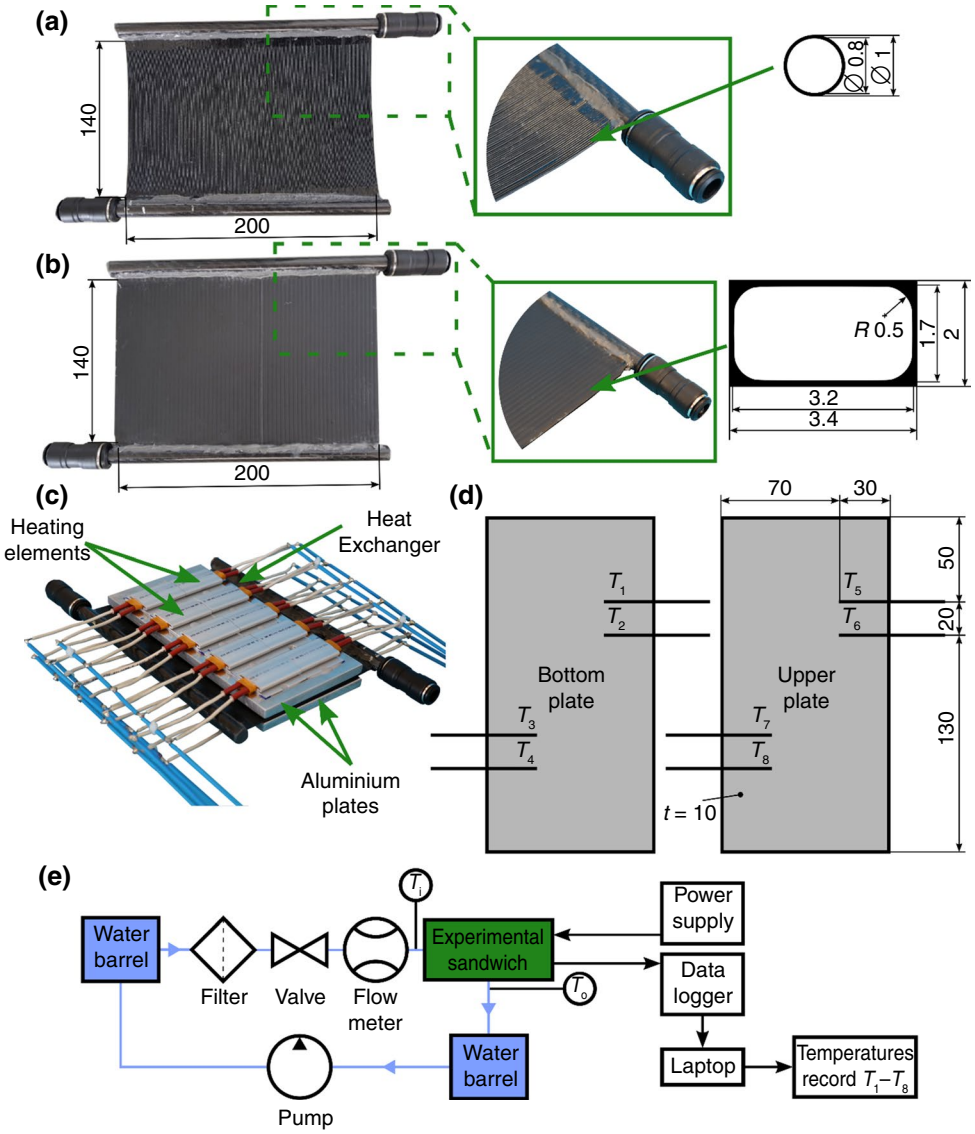

Fig. 1 **a** Polyamide hollow fiber heat exchanger (*F*) with details on the fiber geometry. **b** Polypropylene rectangular curved channels heat exchanger (*C*) with details on its channel geometry. **c** Heat exchanger between aluminum plates with heating elements before placing it into the thermal insulation and positioning thermocouples. After that, this assembly is denoted as an experimental sandwich. **d** Thermocouples positioning. In addition, they are placed in the middle of the plates' thickness. **e** Experimental setup scheme. The pump is used only to relocate water between barrels when needed

surface-to-volume ratio of heat exchangers *F* and *C* is 4000 $m^2\ m^{-3}$ and 964 $m^2\ m^{-3}$. Carbon tubes with an outer diameter of 12 mm were used as the inlet and outlet collectors of both HEs. Momentive's SilCool™ TIA350R Adhesive with a declared thermal conductivity of 3.5 $W\ m^{-1}\ K^{-1}$ was used as an electrically non-conductive gap filler.

The heat exchanger was placed between two 200 × 100×10 mm aluminum plates with heating elements evenly bonded to the plates outside (Fig. 1c). The 30 W power was provided into the electrical circuit using 1685B Series 300–360W Switching Bench DC Power Supplies. The heat exchangers were first tested without the heat-conducting paste, and then, with it, 20 g of heat-conducting paste was applied evenly to each side of the heat exchanger. Eight *K*-type thermocouples were placed in the center of the thickness of the aluminum plates into the drilled holes, four in each, as shown in Fig. 1d, so temperatures could be measured directly at the level of the heating elements and between them. The other two thermocouples measured the temperature at the inlet (T_i) and outlet (T_o) of the distilled water in the heat exchanger, which is the cooling liquid. Distilled water was used to eliminate the fouling of the system.

The plates with heating elements and heat exchanger were placed in insulation—sibral, forming an experimental sandwich. The upper insulation was loaded with a mass of 20 kg to ensure good and well-defined contact between the heat exchanger and the aluminum plates. A PhoenixTM PTM1220-K data logger was used to measure the temperature, which was simultaneously transferred to a laptop, as shown in Fig. 1e. Temperatures were stored when the steady state was reached. The flow rate of the coolant ranged from 1 to 10 l h^{-1}. Four values were measured for the experiments without the paste 1, 2, 4 and 10 l h^{-1} and with the paste 1.3, 2, 4 and 10 l h^{-1}. This flow rate was maintained using a

HAM-LET Group H-1300 series valve, a filter section and a KROHNE flow meter VA40V/R. The exchanger outlet was brought above the inlet level, and the highest possible water flow rate was driven through the exchanger to remove any air or gases present in the system before the measurement started.

The inlet water temperature was maintained at 21 °C, draining by gravity from a barrel above the stand. The experimental scheme setup is shown in Fig. 1e. Due to the low flow rates, the pressure losses were negligibly small. Only numerical calculations estimated the pressure losses. Firstly, a comparison was made between the heat exchangers without paste and those with paste, and the optimal configurations were chosen for both. The main focus was on minimizing the highest recorded temperature within the plates. In the case of experiments, four values are reported in the results (temperature difference, temperature, flow rate and electric power). The uncertainty intervals of these values will now be described. The relative uncertainty of the thermocouple and the data logger is 2.8–7.0% for the measured temperatures in the 20.0–50.0 °C range, corresponding to the absolute error of ± 1.4 °C. The relative error of the measured flow rate is not higher than 5%. The absolute error of the power supply is ± 1.2 W, resulting in a relative error of 4%.

Simulation setup

The numerical model was built to simulate the experiment described in the previous section. Heat is generated uniformly over the entire upper surface of the upper plate and the lower surface of the lower plate, and the inlet temperature of water to all fibers (channels) is constant. Therefore, it is sufficient to consider only one fiber (channel) and the corresponding part of the experimental sandwich in the model. Moreover, since the fibers (channels) are centrally symmetric (see Fig. 1) and the heating bodies are located both above and below, we can advantageously consider only one-quarter of the fiber (channel) and only the upper part of the sandwich. For heat exchanger *F*, the thermally conductive paste is considered, which ensures better contact between the aluminum and the fibers and reduces the maximum temperature in the experiment. On the contrary, in heat exchanger *C*, the thermally conductive paste only brings additional thermal resistance and increases the maximum measured temperature. Therefore, only better options are considered in the simulations. The computational domain for heat exchangers *F* and *C* is shown in Fig. 2a and b. The models were created in Ansys Workbench, and computations were performed in Ansys Fluent (version 2022 R1) with solver SIMPLE.

The mathematical notation of these equations, according to [30], follows. The law of conservation of mass:

$$\nabla \cdot \mathbf{v} = 0, \tag{1}$$

where $\mathbf{v}$ is a velocity vector. The law of conservation of momentum:

$$(\mathbf{v} \cdot \nabla) \cdot \mathbf{v} = -\frac{1}{\rho}\nabla p + \nu \nabla^2 \mathbf{v} \tag{2}$$

where p is the static pressure and ν is the kinematic viscosity. The operator ∇ represents the gradient, and by ∇^2, the Laplace operator is meant. Finally, the law of conservation of energy:

$$\rho c_\mathrm{p}(\mathbf{v} \cdot \nabla T) = \nabla \cdot (k \nabla T) \tag{3}$$

Letter T stands for the temperature, c_p is the specific heat capacity (at the constant pressure) and k is the thermal conductivity. The thermophysical properties of all components are assumed to be constant. Their values are listed in Table 1.

The boundary condition of the heat flux density through the top wall of the aluminum plate is determined to be 750 W m^{-2} (shown as red arrows in Fig. 2), corresponding to the 30 W delivered during experiments to two aluminum plates with an area of 200 × 100 mm. Water at a temperature of 21 °C flows into the fiber (channel) at a rate determined by the flow rate and the cross-sectional area of the fiber (channel). A water flow rate of 1 l h^{-1} corresponds to a velocity of 0.0024 m s^{-1} and 0.00082 m s^{-1} for heat exchangers *F* and *C*, respectively. The boundary condition at the fiber (channel) outlet is chosen as a pressure outlet with a value of 0 Pa. At the point of contact between the water and the fiber (channel) wall, the no-slip condition is set. Other interferences between the bodies are set as coupled, and perfect thermal contact is considered. The system is isolated from the surrounding environment. A symmetry condition is prescribed at the boundary between the water and the surroundings.

Concerning the meshing of domains, the aim is to keep the skewness of the cells as small as possible. Although an ideal scenario would have entailed a zero-thickness layer of thermally conductive paste at the narrowest point (concerning the case with heat exchanger *F*), the formation of cells with excessive skewness can lead to computation convergence issues was avoided using a 0.03 mm thickness instead. As a result, the maximum skewness in both models was limited to 0.75, with a mean value of approximately 0.06 in both cases, see Table 2. The inflation mesh method created a finer mesh at the interface between the water and the fiber wall to better capture the boundary layer region where temperature and velocity changes occur. Although a large aspect ratio is typically undesirable, it was possible to use in this case due to the highly anisotropic flow inside the fiber (channel). As a result, the number of cells required was significantly

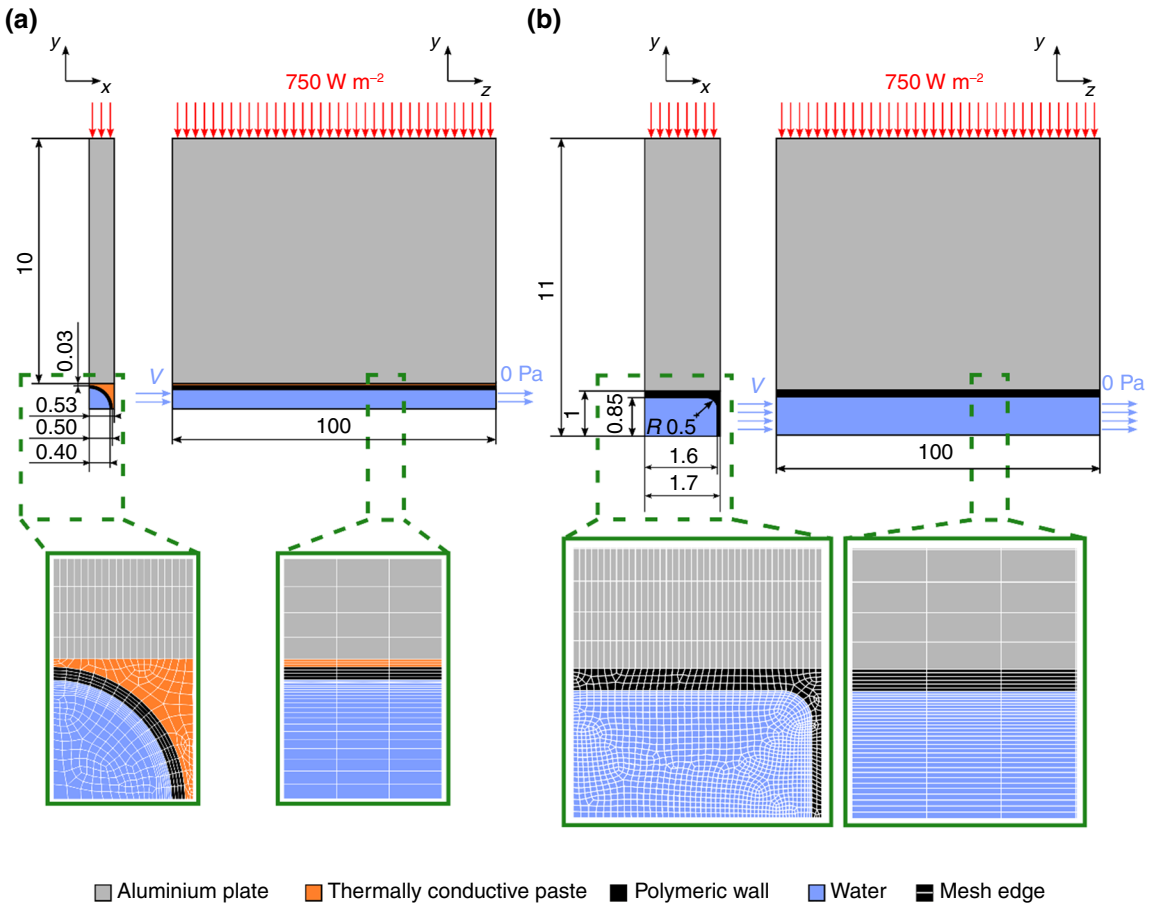

Fig. 2 Simulations domains for the case with **a** polyamide hollow fiber heat exchanger (*F*) and **b** polypropylene rectangular curved channels heat exchanger (*C*), illustration of boundary conditions, and details of used mesh grids

reduced without compromising the accuracy of the results. The overall number of cells was around 490 000 in both cases. Details of the meshes are displayed in Fig. 2.

Results

Workflow

The procedure of the work itself is divided into two stages: (1) In the Ansys Fluent environment, create a model so that the results of the simulations are as close as possible to the reality measured in the experiment described in the experimental section. The measured values of the maximum temperature in the aluminum plates and the water temperature at the outlet of the fiber (channel) differ at most 10% from the corresponding values predicted by the simulations. (2) Substitute the material properties of the aluminum plate for the pouch battery (Table 1), including consideration of anisotropy, and compare the plastic variants from the first stage with heat exchangers made of aluminum, keeping the same geometry.

The comparison of the simulation prediction with experiments for heat exchanger *F* (left column) and *C* (right column) for the maximum temperature (Fig. 3) shows an error of up to 5% (or up to 11%) for *F* (or *C*), indicating good accuracy. Similar observations hold for the outlet water temperature. Based on the calculations and data above, the model accurately describes the experiment and can be utilized in subsequent parameter studies. The maximal temperature from the simulation is taken as the temperature in the middle of the thickness and width of the aluminum plate and 30 mm from the outlet, so it is the exact location as in the experimental case.

Replacement of the aluminum plate with a pouch battery

Two additional models were created using ANSYS FLUENT, with the same geometry as in the previous stage but

Table 1 Thermophysical properties of aluminum, thermally conductive paste, polyamide, polypropylene, water and a pouch battery

Aluminum [31]	ρ	2702	(kg m^{-3})
	c_p	903	(J kg^{-1}K^{-1})
	k	237	(W m^{-1} K^{-1})
Thermally conductive paste [32]	ρ	3100	(kg m^{-3})
	c_p	1100	(J kg^{-1} K^{-1})
	k	3.5	(W m^{-1} K^{-1})
Polyamide [33]	ρ	1140	(kg m^{-3})
	c_p	1700	(J kg^{-1}K^{-1})
	k	0.23	(W m^{-1} K^{-1})
Polypropylene [34]	ρ	895	(kg m^{-3})
	c_p	1920	(J kg^{-1}K^{-1})
	k	0.19	(W m^{-1}K^{-1})
Water [31]	ρ	997.86	(kg m^{-3})
	c_p	4179	(J kg^{-1}K^{-1})
	k	0.613	(W m^{-1}K^{-1})
	ν	$0.855\,10^{-6}$	(m^2 s^{-1})
Battery [35]	ρ	2510	(kg m^{-3})
	c_p	990	(J kg^{-1}K^{-1})
	k	$\begin{bmatrix} 39.9 & 0 & 0 \\ 0 & 1.19 & 0 \\ 0 & 0 & 39.9 \end{bmatrix}$	(W m^{-1}K^{-1})

with aluminum fiber (channel) material instead of polymeric. We compared three parameters: the maximum temperature, the water outlet temperature and the temperature difference in the aluminum plate. The plates' thermophysical properties were replaced with batteries to make the simulations closer to reality. The anisotropy of the battery was specified in the form of a tensor, and the thermophysical properties are listed in Table 1. A significant difference was observed between the models with batteries and those with aluminum plates. The thermal conductivity in the y-axis direction was more than 30 times smaller than in the other two directions, resulting in a higher maximum temperature and a change in the temperature profile. The temperature field in the case of the plastic heat exchanger F with a flow rate of 1.3 l h^{-1} with the replacement of the aluminum by a battery is shown in Fig. 4d. The values of the maximum temperature, the outlet water temperature and the maximum difference inside the battery are shown in Fig. 5. The relative differences between the aluminum and the plastic variants were most significant for exchanger C at a flow rate of 10 l h^{-1}, with the maximum temperature difference of the polymeric variant being almost 12% lower. However, the absolute difference was less than 0.1 °C, i.e., negligible. This is attributed to the fiber material's significantly lower thermal resistance in comparison with other thermal resistances. Due to the laminar flow and low water velocity values, the heat transfer coefficient (HTC) of the heat exchangers is significantly not dependent on the flow rate. Thus, only mean values will be stated. The HTC of the heat exchanger C was 842.89 W m^{-2} K^{-1} for polymeric channels and 877.61 W m^{-2} K^{-1} for the aluminum ones, leading to an increase of circa 4% for the latter case. A higher HTC can be observed for the heat exchanger F due to the smaller inner diameter, i.e., 2691.46 W m^{-2} K^{-1} for polymeric fibers and 2765.48 W m^{-2} K^{-1} for aluminum ones.

Table 2 Number of cells used for models considering heat exchangers F and C. Selected mesh parameters used in the models: skewness and aspect ratio of cells. For each parameter, the interval (I) over which the values occur, the mean) and the standard deviation (σ) of the parameter are specified

Amount of cells		Skewness			Aspect ratio		
		I	μ	σ	I	μ	σ
F	492 000	0–0.71	0.060	0.12	3.68–35.49	14.33	8.04
C	487 600	0–0.51	0.058	0.092	10.23–53.43	16.55	6.26

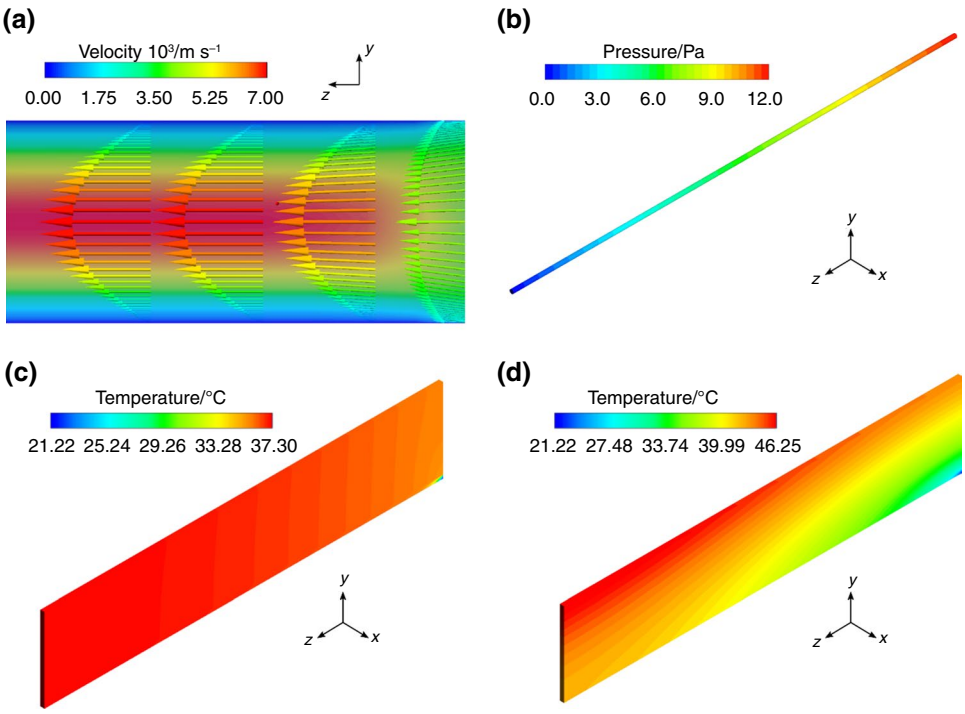

Fig. 3 Results of simulation for the case with heat exchanger *F* with a flow rate of 1.3 l h^{-1}: **a** water velocity profile inside the fiber and velocity vectors at several positions, viewed in the *yz* plane in the middle of the fiber, **b** computed pressure along the fiber, **c** temperature distribution in the computational domain and **d** temperature distribution in the domain with aluminum thermophysical properties replaced with the batteries

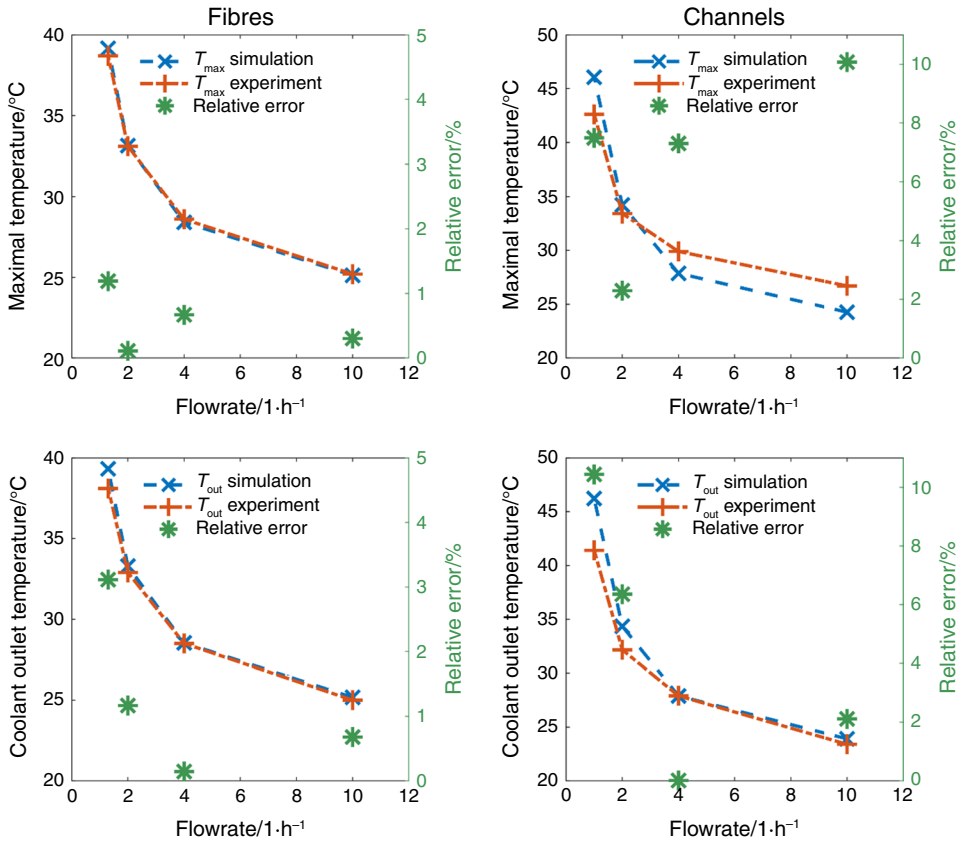

Fig. 4 Comparison of maximal temperature and coolant outlet temperature during simulations (blue) and experiments (red) with heat exchangers *F* (left column) and *C* (right column). Thermophysical properties of aluminum were considered for cooled plates

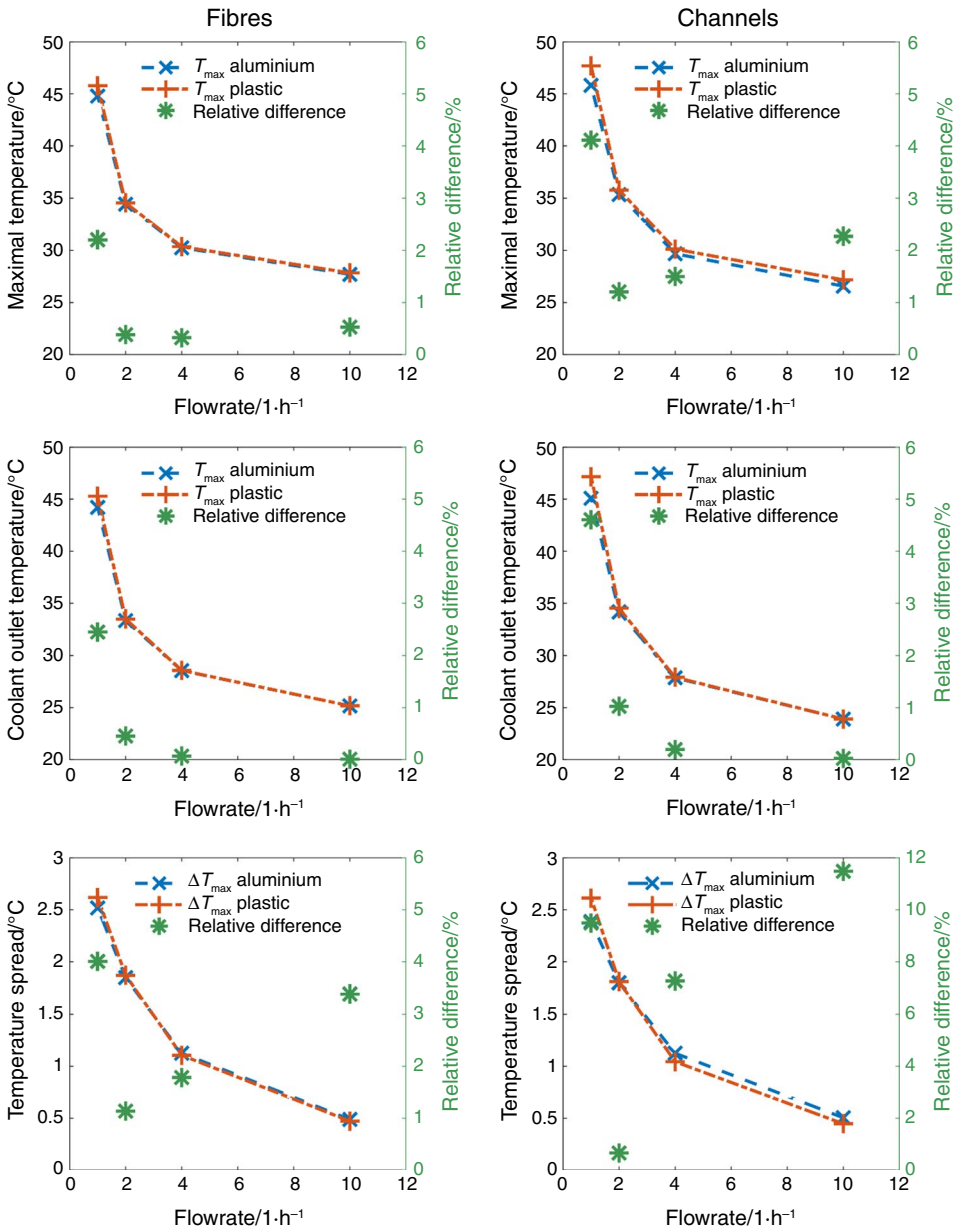

Fig. 5 Comparison of maximal temperature, coolant outlet temperature and maximal temperature during simulations with heat exchangers *F* (left column) and *C* (right column) from polymeric materials (red) and aluminum (blue). Thermophysical properties of the battery were considered for cooled plates

Conclusions

Experiments were performed to compare two types of heat exchangers for cooling flat elements with an emphasis on batteries. These are polymeric heat exchangers, one made of polymeric hollow fibers (*F*) and the other made of plastic cardboard (*C*) with rectangular channels with rounded corners. The heat exchangers were placed between two aluminum plates, to which a power of 30 W was applied. Water flowed (1–10 l h^{-1}) through the fibers (channels), and the temperature inside plates were monitored at several positions. The results showed that applying a thermally conductive paste to the *F* exchanger is necessary. In contrast, the application of paste to the *C* exchanger only brings additional thermal resistance and thus leads to worse thermal performance.

The experimental data further validated the computational model, which was also conscientiously verified. The *F* and *C* heat exchangers were compared in polymeric and aluminum versions with the same geometry in simulations. It is important to note that the thermophysical properties of the battery are fundamentally different from aluminum. This is mainly the anisotropy of thermal conductivity. In the case of including anisotropy in the model, where the thermal conductivity is more than 30 times smaller in the direction perpendicular to the heat exchangers than in the other two directions, minor differences were observed between the polymeric and aluminum variants in terms of

maximum temperatures and temperature differences across the battery. The *F* heat exchanger exhibited a higher heat transfer coefficient (2691.46 W m^{-2} K^{-1}) attributed to the smaller inner diameter of its fibers, while the heat transfer coefficient for the *C* exchanger was 877.61 W m^{-2} K^{-1}. Importantly, replacing the polymeric wall with an aluminum one yielded only a marginal increase in heat transfer coefficient, not exceeding 5%.

In addition, the polymeric exchangers are not electrically conductive and, therefore, do not need to be electrically isolated from the batteries, as with the aluminum exchangers. They also bring the advantages of lower mass, cheaper manufacturing material and lower carbon footprint per unit mass. Research and development in polymeric heat exchangers will grow with interest in electromobility, where properly designed thermal management plays an essential role.

In current electric vehicles, battery thermal management systems do not optimize the coolant flow rate. Usually, two states occur: (1) Either there is no need to cool (driving at reasonable speeds without much acceleration), or (2) there is a great need to cool (charging, significant acceleration). Therefore, if the vehicle is actively cooling the battery, it does so with high flow rates. We have shown that at higher flow rates, we do not observe a significant difference in maximal temperature between the polymeric and aluminum versions of the heat exchangers. Moreover, the plates with the polymeric variant have a lower temperature difference. Currently, the main drawback of plastic exchangers is their higher price due to mass production limitations. In future work, the design of the PCPHE will be provided. The overall channel dimensions and wall thicknesses will be optimized to ensure solid mechanical stability of the system while maintaining good thermal performance. Moreover, tests with actual batteries of different types will be performed to validate more sophisticated computational models.

Acknowledgements This work was supported by the internal grant of the Brno University of Technology focused on specific research and development No. FSI-S-23-8254.

Author contributions Jiri Hvozda contributed to conceptualization, methodology, writing—original draft and writing—review and editing. Krystof Mraz contributed to the investigation and writing—review and editing. Miroslav Raudensky contributed to supervision and writing—review and editing. Alexander Vakhrushev contributed to methodology and writing—review and editing. Ebrahim Karimi-Sibaki contributed to methodology and writing—review and editing. Jan Bohacek contributed to conceptualization and writing—review and editing.

Funding Open access publishing supported by the National Technical Library in Prague.

Data availability The data supporting this study's findings are available on request from the corresponding author.

Declarations

Conflict of interest The authors declare that they have no known competing financial interests or personal relationships that could have appeared to influence the work reported in this paper.

Open Access This article is licensed under a Creative Commons Attribution 4.0 International License, which permits use, sharing, adaptation, distribution and reproduction in any medium or format, as long as you give appropriate credit to the original author(s) and the source, provide a link to the Creative Commons licence, and indicate if changes were made. The images or other third party material in this article are included in the article's Creative Commons licence, unless indicated otherwise in a credit line to the material. If material is not included in the article's Creative Commons licence and your intended use is not permitted by statutory regulation or exceeds the permitted use, you will need to obtain permission directly from the copyright holder. To view a copy of this licence, visit http://creativecommons.org/licenses/by/4.0/.

References

1. International Energy Agency. Global EV Outlook 2021 [online]. ©IEA 2021 [cit. 15. 7. 2023]. Available at: https://www.iea.org/reports/global-ev-outlook-2021.
2. International Energy Agency. Global EV Outlook 2022 [online]. ©IEA 2022 [cit. 15. 7. 2023]. Available at: https://www.iea.org/reports/global-ev-outlook-2022.
3. Herrmann F, Rothfuss F. Advances in battery technologies for electric vehicles. Sawston: Woodhead Publishing; 2015.
4. Omar N, et al. Standardization work for BEV and HEV applications: critical appraisal of recent traction battery documents. Energies. 2012;5(12):138–56. https://doi.org/10.3390/en5010138.
5. Yue QL, He CX, Wu MC, Zhao TS. Advances in thermal management systems for next-generation power batteries. Int J Heat Mass Transf. 2021;181:121853. https://doi.org/10.1016/j.ijheatmasstransfer.2021.121853.
6. Rao Z, Wang S. A review of power battery thermal energy management. Renew Sustain Energy Rev. 2011;15(9):4554–71. https://doi.org/10.1016/j.rser.2011.07.096.
7. Hamed MM, El-Tayeb A, Moukhtar I, el Dein AZ, Abdelhameed EH. A review on recent key technologies of lithium-ion battery thermal management: external cooling systems. Res Eng. 2022;16:100703. https://doi.org/10.1016/j.rineng.2022.100703.
8. Zhang X, Li Z, Luo L, Fan Y, Du Z. A review on thermal management of lithium-ion batteries for electric vehicles. Energy. 2022;238:121652. https://doi.org/10.1016/j.energy.2021.121652.
9. Luo J, Zou D, Wang Y, Wang S, Huang L. Battery thermal management systems (BTMs) based on phase change material (PCM): a comprehensive review. Chem Eng J. 2022;430(1):132741. https://doi.org/10.1016/j.cej.2021.132741.
10. Bernagozzi M, Georgoulas A, Miche N, Marengo M. Heat pipes in battery thermal management systems for electric vehicles: a critical review. Appl Therm Eng. 2022;219:119495. https://doi.org/10.1016/j.applthermaleng.2022.119495.
11. Sun Z, Guo Y, Zhang C, Whitehouse J, Zhou Q, Xu H, Wang C. Experimental study of battery passive thermal management system using copper foam-based phase change materials. Int J Thermofluids. 2022;17:100255. https://doi.org/10.1016/j.ijft.2022.100255.
12. Ghaeminezhad N, Wang Z, Ouyang Q. A review on lithium-ion battery thermal management system techniques: a control-oriented

analysis. Appl Therm Eng. 2022;219:119497. https://doi.org/10.1016/j.applthermaleng.2022.119497.
13. Li Y, Guo H, Qi F, Guo Z, Li M, Tjernberg LB. Investigation on liquid cold plate thermal management system with heat pipes for $LiFePO_4$ battery pack in electric vehicles. Appl Therm Eng. 2021;185:116382. https://doi.org/10.1016/j.applthermaleng.2020.116382.
14. Chen F, et al. Air and PCM cooling for battery thermal management considering battery cycle life. Appl Therm Eng. 2020;173:115154. https://doi.org/10.1016/j.applthermaleng.2020.115154.
15. Wu X, et al. Experimental and numerical study on hybrid battery thermal management system combining liquid cooling with phase change materials. Int Commun Heat Mass Transf. 2022;139:106480. https://doi.org/10.1016/j.icheatmasstransfer.2022.106480.
16. Peng P, Wang Y, Jiang F. Numerical study of PCM thermal behavior of a novel PCM-heat pipe combined system for Li-ion battery thermal management. Appl Therm Eng. 2022;209:118293. https://doi.org/10.1016/j.applthermaleng.2022.118293.
17. Wazeer A, Das A, Abeykoon C, Sinha A, Karmakar A. Phase change materials for battery thermal management of electric and hybrid vehicles: a review. Energy Nexus. 2022;7:100131. https://doi.org/10.1016/j.nexus.2022.100131.
18. Xiujuan Y, et al. Analysis of improved novel hollow fiber heat exchanger. Appl Therm Eng. 2014;671–2:114–21.
19. Hussain AR, et al. Review of polymers for heat exchanger applications: factors concerning thermal conductivity. Appl Therm Eng. 2017;113:1118–27.
20. Bohacek J, Hvozda J, Mraz K, Vakhrushev A, Karimisibaki E. Polymeric hollow fibers: a modular heat exchanger for thermal management systems of battery modules in electric vehicles. In: EFM21—15th International conference "experimental fluid mechanics 2021. November 23–26, 2021, Liberec, Czechia. Les Ulis: EPJ Web of Conferences, 2022, p. 01005. doi: https://doi.org/10.1051/epjconf/202226401005.
21. The greenhouse gases, regulated emissions, and energy use in technologies (GREET®) Model. [Computer software]. Version 2021, Argonne National Laboratory. Available at: https://greet.es.anl.gov/.
22. Zarkadas DM, Sirkar K. Polymeric hollow fiber heat exchangers: an alternative for lower temperature applications. Ind Eng Chem Res. 2004;43(25):8093–106. https://doi.org/10.1021/ie040143k.
23. Bohacek J, Raudensky M, Kroulikova T. Polymeric hollow fibers: a supercompact cooling of Li-ion cells. Int J Therm Sci. 2019;146:106060. https://doi.org/10.1016/j.ijthermalsci.2019.106060.
24. Bohacek J, Raudensky M, Karimi-Sibaki E. Polymeric hollow fibers: uniform temperature of Li-ion cells in battery modules. Appl Therm Eng. 2019;159:113940. https://doi.org/10.1016/j.applthermaleng.2019.113940.
25. Kudelova T, et al. Fully polymeric distillation unit based on polypropylene hollow fibers. Polymers. 2021;13(7):1031. https://doi.org/10.3390/polym13071031.
26. Kroulikova T, et al. Comparison of a novel polymeric hollow fiber heat exchanger and a commercially available metal automotive radiator. Polymers. 2021;13(7):1175. https://doi.org/10.3390/polym13071175.
27. Kroulikova T, et al. Heat exchanger for air-liquid application with chaotised polymeric hollow fibers. Appl Therm Eng. 2021;197:117365. https://doi.org/10.1016/j.applthermaleng.2021.117365.
28. Mraz K, et al. Case study of liquid cooling of automotive headlights with hollow fiber heat exchanger. Case Stud Therm Eng. 2021;28:101689. https://doi.org/10.1016/j.csite.2021.101689.
29. Sirková BK, et al. Polymeric hollow fiber heat transfer surface for heat exchanger. Appl Therm Eng. 2023;233:121120. https://doi.org/10.1016/j.applthermaleng.2023.121120.
30. Moukalled FH, Mangani L Darwish M (2016) The finite volume method in computational fluid dynamics: an advanced introduction with OpenFOAM® and Matlab®. Springer: Cham
31. Bergman TL, Incropera FP, Dewitt DP, Lavine AS. Fundamentals of heat and mass transfer. 7th ed. Hoboken: Wiley; 2011.
32. Momentive. SilCool™ TIA350R Adhesive [online]. ©Momentive 2023 [cit. 15. 7. 2023]. Available at: https://www.momentive.com/en-us/categories/adhesives-and-sealants/silcool-tia350radhesive.
33. Polyplasty. Polyamide [online]. ®Polyplasty 2023 [cit. 15. 7. 2023]. Available at: https://www.polyplasty.cz/material-polyamid.html?lang=2.
34. Gahleitner M, Paulik C. Polypropylene. Ullmann's encyclopedia of Industrial. Chemistry. 2000. https://doi.org/10.1002/14356007.o21_o04.pub2.
35. Maleki H, et al. Li-Ion polymer cells thermal property changes as a function of cycle-life. J Power Sources. 2014;263:223–30. https://doi.org/10.1016/j.jpowsour.2014.04.033.

Publisher's Note Springer Nature remains neutral with regard to jurisdictional claims in published maps and institutional affiliations.